第 46 卷 第 6 期 质 谱 学 报 Vol. 46 No. 6
2025 年 11 月 Journal of Chinese Mass Spectrometry Society Nov. 2025

Unraveling Single-Cell Metabolic Features in Breast Cancer Drug Resistance Using Mass Spectrometry

LIU Chun-yan[1], CHEN Hao-ran[1], WANG Yan[1], WU Xian-zhe[1], FANG Dan-jun[1], CHEN Yun[1,2,3,4,5]

(1. *School of Pharmacy*, *Nanjing Medical University*, *Nanjing* 211166, *China*;
2. *State Key Laboratory of Reproductive Medicine and Offspring Health*, *Nanjing Medical University*, *Nanjing* 211166, *China*; 3. *Key Laboratory of Cardiovascular & Cerebrovascular Medicine*, *Nanjing Medical University*, *Nanjing* 211166, *China*; 4. *Innovation Center of Suzhou*, *Nanjing Medical University*, *Suzhou* 215000, *China*;
5. *National Center of Technology Innovation for Biopharmaceuticals*, *Suzhou* 215000, *China*)

Abstract: Drug resistance remains a major challenge in breast cancer chemotherapy, yet the metabolic alterations underlying this phenomenon are not fully understood. There is much evidence indicating the cellular heterogeneity among cancer cells, which exhibit varying degrees of metabolic reprogramming and thus may result in differential contributions to drug resistance. A home-built single-cell quantitative mass spectrometry (MS) platform, which integrates micromanipulation and electro-osmotic sampling, was developed to quantitatively profile the tricarboxylic acid (TCA) cycle metabolites at the single-cell level. Using this platform, the metabolic profiles of drug-sensitive MCF-7 breast cancer cells and their drug-resistant derivative MCF-7/ADR cells were compared. This results revealed a selective upregulation of downstream TCA cycle metabolites including α-ketoglutarate, succinate, fumarate, and malate in drug-resistant cancer cells, while early TCA metabolites remained largely unchanged. Furthermore, notable variations in the abundance of the metabolites were observed in individual cells. The comparative analysis also revealed that not all MCF-7/ADR cells exhibit the same degree of metabolic deviation from the parental line in the metabolites during resistance acquisition. The observed metabolic profiles indicate enhanced glutaminolysis, altered mitochondrial electron transport chain activity, and increased metabolic flexibility in drug-resistant cancer cells that support their survival under chemotherapeutic stress. The findings further suggest the potential for incorporating cellular metabolic heterogeneity into future drug resistance studies.

Key words: mass spectrometry; single-cell metabolic features; breast cancer drug resistance; tricarboxylic acid (TCA) cycle

CLC number: O657.63 **Document code:** A **Article ID:** 1004-2997(2025)06-0826-12

DOI: 10.7538/zpxb.2025.0092 **CSTR:** 32365.14.zpxb.2025.0092

This work was supported by National Natural Science Foundation of China (22374080, 22174068, 21722504); Primary Research & Development Plan of Jiangsu Province (BK20221303, BE2022796); Open Foundation of State Key Laboratory of Reproductive Medicine (SKLRM-2022BP1, JX116GSP20240507); Science and Technology Development Fund of NJMU (NJMUQY2022003)

LIU Chun-yan and CHEN Hao-ran contribute equally to this article

Correspondence: CHEN Yun, FANG Dan-jun

单细胞质谱技术揭示乳腺癌耐药的代谢特征

刘春艳[1]，陈浩然[1]，王　妍[1]，武贤哲[1]，方丹君[1]，陈　芸[1,2,3,4,5]

（1. 南京医科大学药学院，江苏 南京　211166；2. 南京医科大学，生殖医学与子代健康全国重点实验室，江苏 南京　211166；3. 南京医科大学，心脑血管药物研究重点实验室，江苏 南京　211166；4. 南京医科大学苏州创新中心，江苏 苏州　215000；5. 国家生物医药技术创新中心，江苏 苏州　215000）

摘要：耐药性是乳腺癌化疗的主要挑战之一，其背后的代谢机制尚未被充分阐明。研究表明，细胞间存在显著的异质性，不同细胞表现出的代谢重编程程度不同，这可能导致其对药物反应的差异。本研究构建了一套集显微操作与电渗采样于一体的单细胞定量质谱分析平台，可在单细胞水平上定量分析三羧酸（TCA）循环代谢物。利用该平台比较了药物敏感型乳腺癌细胞 MCF-7 与其耐药株 MCF-7/ADR 的代谢特征。结果表明，在耐药细胞中，TCA 循环的下游代谢物（包括 α-酮戊二酸、琥珀酸、延胡索酸和苹果酸）显著增加，而早期代谢物变化不大。此外，不同单细胞间代谢物丰度存在明显差异。本研究还发现，并非所有 MCF-7/ADR 细胞在耐药性形成过程中都呈现相同程度的代谢偏离。上述代谢特征表明，耐药性癌细胞会通过加强谷氨酰胺分解、调节线粒体电子传递链的活性以及提升自身的代谢灵活性，以维持其在药物应激下的存活。因此，将细胞代谢异质性纳入未来的耐药性研究具有潜在的研究价值。

关键词：质谱；单细胞代谢特征；乳腺癌耐药性；三羧酸（TCA）循环

Breast cancer remains one of the most prevalent malignancies among women worldwide, with persistently high incidence rates that continue to pose serious challenges to women's health and survival[1-2]. Despite the availability of diverse treatment options, including surgery, radiotherapy, chemotherapy, endocrine therapy, and targeted therapies, chemotherapy continues to serve as a cornerstone in breast cancer management[3-4].

Among the widely used chemotherapeutic agents, doxorubicin (DOX) is a key component of many first-line treatment regimens due to its broad antitumor spectrum and proven clinical efficacy[5-6]. However, the therapeutic benefits of DOX are often short-lived, as cancer cells tend to develop drug resistance over time[7-8]. This acquired resistance is a major contributor to treatment failure, disease recurrence, and distant metastasis, ultimately compromising patient outcomes.

In recent years, metabolic reprogramming has emerged as a process associated with drug resistance in cancer development[9-10]. Specifically, cancer cells frequently undergo metabolic adaptation to survive in hostile environments imposed by drug treatment[11]. Among the key metabolic pathways involved, the tricarboxylic acid (TCA) cycle plays a central role not only in energy production but also in the biosynthesis of macromolecules and the maintenance of redox balance. It involves several key metabolites, including citrate, isocitrate, α-ketoglutarate, aconitate, succinate, fumarate, malate, and oxaloacetate, which support both energy metabolism and anabolic processes[12-14]. Increasing evidence suggests that drug-resistant cancer cells may upregulate TCA cycle activity to meet heightened energy demands or reroute metabolic fluxes to evade apoptosis[15-16]. More importantly, individual cells exhibit varying degrees of metabolic reprogramming, resulting in differential contributions to drug resistance[17]. However, most current studies of cancer metabolism come from bulk-level analyses[18-19], which obscure the cellular metabolic heterogeneity within tumors and limit our understanding of resistance mechanisms at the single-cell level.

Mass spectrometry (MS), owing to its high sensitivity and specificity, has been extensively applied and has rapidly progressed in the field of single-cell metabolomics[20-21]. Compared with conventional single-cell analytical techniques such as electrochemical sensing and fluorescence-based

assays[22-23], MS can simultaneously quantify a wide range of metabolites in a single run and enable structural characterization *via* tandem mass spectrometry (MS/MS), thereby establishing itself as a powerful platform in omics research. More importantly, electrospray ionization (ESI)-based single-cell MS techniques have been widely developed and provided powerful tools for single-cell metabolomics research[24-27]. Our lab has previously established a home-built single-cell quantitative MS platform for metabolomics analysis in cells[28].

In this study, we investigated the metabolic heterogeneity underlying breast cancer drug resistance by using DOX-sensitive MCF-7 breast cancer cells and their DOX-resistant derivative, MCF-7/ADR cells. We further developed single-cell quantitative MS platform to profile metabolic features of the TCA cycle. Key TCA metabolites including citrate, isocitrate, *α*-ketoglutarate, succinate, fumarate, and malate were quantified at the single-cell level. Comparative analysis between breast cancer drug-sensitive and resistant cell populations was carried out to reveal the metabolic alterations associated with drug resistance acquisition.

1 Methods

1.1 Chemicals and Reagents

Metabolite reagents, including citrate, isocitrate, *α*-ketoglutarate, succinate, fumarate, and malate were purchased from Aladdin (Shanghai, China). 1-Butanol, LC-MS grade methanol and bovine serum albumin (BSA) were obtained from Sigma-Aldrich (St. Louis, USA). Borosilicate glass capillaries (BF100-58-10) were purchased from Sutter Instrument (Novato, USA). 4-Acetaminophen was supplied by Aladdin (Shanghai, China). Ammonium acetate was purchased from Sinopharm Chemical Reagent (Shanghai, China). Fetal bovine serum (FBS), Dulbecco's Modified Eagle Medium (DMEM) and penicillin/streptomycin solution were obtained from Thermo Scientific HyClone (Logan, USA).

1.2 Preparation of Stock Solutions

In this experiment, the concentration of each metabolite and internal standard in stock solution was 50 mmol/L. 4-Acetaminophen was used as the internal standard because it is not naturally present in cells or biological systems. All solutions were stored at −20 ℃ in brown glass tubes to keep them away from light and thawed to room temperature before use. In this study, a series of calibration standards were prepared. The lower limit of quantification (LLOQ) was used as a quality control (QC) criterion, and three independent validation experiments were conducted on separate days. Each experiment included a calibration curve measured in duplicate and 6 QC samples, resulting in a total of 18 QC data points.

1.3 Cell Culture and Collection

MCF-7 (Cell Resource Center of the Chinese Academy of Medical Sciences, Shanghai, China) and MCF-7/ADR cells (Keygen Biotech, Nanjing, China) were cultured in DMEM supplemented with 10% FBS and 1% penicillin/streptomycin at 37 ℃ in 5% CO_2. The cells were passaged every 5 days using 0.25% trypsin. To maintain a highly drug-resistant cell population, MCF-7/ADR cells were periodically reselected by growing them in the presence of 1 000 μg/L DOX. In addition, MCF-7/ADR cells exhibited evident morphological changes compared with the parental MCF-7 cells[29]. Finally, the culture medium was removed, and the cells were washed three times with PBS and resuspended in PBS to facilitate subsequent single-cell collection.

1.4 Capillary Preparation for Single-cell Manipulation

Single-cell manipulation was performed using nanopipettes fabricated from borosilicate glass capillaries (inner diameter of 0.58 mm, outer diameter of 1 mm, with filament). These nanopipettes, which also served as emitters for ionization during MS analysis, were prepared using a Sutter P-2000 puller (Sutter Instrument, Novato, USA) with the following two-step program: first, HEAT=350, FIL=3, VEL=30, DEL=220, PULL=NA; followed by

HEAT=350, FIL=3, VEL=40, DEL=180, PULL=120. The resulting nanopipettes were subsequently characterized by scanning electron microscopy (SEM, JSM 7800F, JEOL Ltd., Tokyo, Japan) to verify their structural integrity.

1.5 Single-cell Micro-sampling

For single-cell manipulation, the nanopipette was precisely controlled using a motorized micromanipulation system (NTX-N4, Nikon, Tokyo, Japan) mounted on an inverted microscope (Ti2-U, Nikon, Tokyo, Japan). An Ag/AgCl wire, serving as the working electrode, was inserted into the nanopipette and connected to an electrochemical workstation (CHI 660, CH Instruments, Austin, USA). Another Ag/AgCl wire was employed as the reference electrode to establish a complete electrical circuit, enabling electro-osmosis-assisted cellular extraction. Before cell sampling, the capillary was filled with electrolyte solution (1-butanol solution containing 40 mmol/L ammonium acetate) to extract cellular contents, followed by the sequential extraction of approximately 190 fL of a 100 mg/L internal standard solution. Following extraction, the nanocapillary tip was positioned approximately 5 mm from the inlet of the mass spectrometer for subsequent analysis.

1.6 MS Analysis

Detection of target molecules was carried out using a SCIEX QTRAP 5500 MS/MS system. Multiple reaction monitoring (MRM) transitions were individually optimized for each analyte. The MS parameters were set as follows: curtain gas (CUR) was set to 10, and ion spray voltage (IS) was set to –2 000 V under negative ion mode and +2 000 V under positive ion mode.

1.7 Western Blotting

Cells were lysed using RIPA lysis buffer and quantified by BCA Protein Quantification Kit (P0009, Beyotime, Shanghai, China). The proteins were resolved using 12% SDS-PAGE and transferred to a PVDF membrane (0.45 μm, Merck, Germany). The membrane was blocked with 5% normal goat serum (C0265, Beyotime, Shanghai, China) for 2 h and then incubated with the primary antibodies against target proteins at 4 ℃ overnight: IDH1 (Mouse, 1:1 000, 66197-1-Ig, Proteintech, China), GLS (Rabbit, 1:5 000, 12855-1-AP, Proteintech, China), GAPDH (Mouse, 1:50 000, 60004-1-Ig, Proteintech, China). Afterward, the membrane was washed, followed by incubated with secondary antibodies: HRP-conjugated Goat Anti-Mouse IgG(H+L) (1:10 000, SA00001-1, Proteintech, China), HRP-conjugated Goat Anti-Rabbit IgG(H+L) (1:10 000, SA00001-2, Proteintech, China), and then detected by ECL-chemiluminescence (P0018FS, Beyotime, Shanghai, China). The experiments were repeated three times, and the results were normalized to GAPDH.

1.8 Data Analysis

For each metabolite, the peak area was normalized by calculating the ratio to the internal standard peak area, in order to reduce variation and allow for the comparison across samples. MetaboAnalyst (http://www.metaboanalyst.ca) was used to calculate the sample size in this study. The sample size was estimated at a false discovery rate (FDR) threshold of 0.01 and a statistical efficacy of 90%, based on the abundance of the target metabolites. Hierarchical clustering heatmap analysis was performed using the online Hiplot platform (https://hiplot.com.cn). Principal component analysis (PCA) was carried out using R package (https://github.com/CHR-njmu/PCA). Other plots were generated using GraphPad Prism 9.0.

2 Results and Discussion

2.1 Establishment of a Home-built MS-based Single-cell Platform

In this study, we employed a home-built MS-based single-cell platform that integrates micromanipulation, electro-osmotic sampling, and ESI-based MS to achieve *in situ* extraction and direct detection of intracellular metabolites. The core of this method lies in the use of a pulled glass nanocapillary to precisely penetrate individual cells under microscopic guidance, allowing for quantitative

extraction of cellular contents. The extracted analytes are then directly introduced into the mass spectrometer via ESI (Fig.1). It offers high specificity, quantitative capability, and does not require any labeling or derivatization.

Specifically, glass capillaries were pulled using a laser-based micropipette puller to form nanopipettes with tip diameters of approximately 220 nm (Fig.2a and 2b). The tip was carefully inserted into target single cells under the control of a micromanipulator. Upon applying a moderate voltage to the rear end of the capillary, electro-osmotic flow was induced, facilitating the migration of intracellular fluid into the capillary, with extraction volumes reaching the femtoliter scale. Theoretically, the extracted volume is primarily governed by the applied voltage and the duration of application. The volume was estimated based on the angle "α" between the cone-shaped tip and its axis, the observed diameter "a", and the height "h" of the meniscus formed between the hydrophobic electrolyte and the extracted aqueous phase, calculated using the following formula $V = \frac{\pi a^3}{3\tan\alpha}\left((1+L\tan\alpha)^3 - 1\right)$, $L = \frac{h}{a}$ (Fig.2c)[28,30]. Experimental results were consistent with this theoretical prediction: at a fixed extraction time of 40 s, the extracted volume increased linearly with applied voltages ranging from 0 V to –4 V (Fig.2d). Conversely, under a constant voltage of –2 V, the volume showed a proportional increase with extraction times between 20 s and 100 s (Fig.2e). Considering extraction efficiency and cell viability,

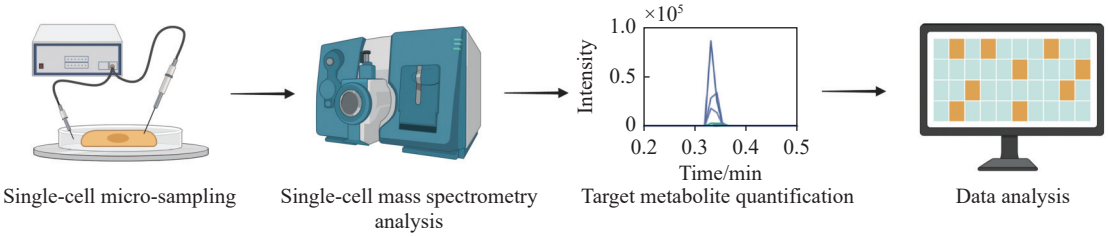

Fig. 1 Workflow diagram of the single-cell quantitative MS analysis platform

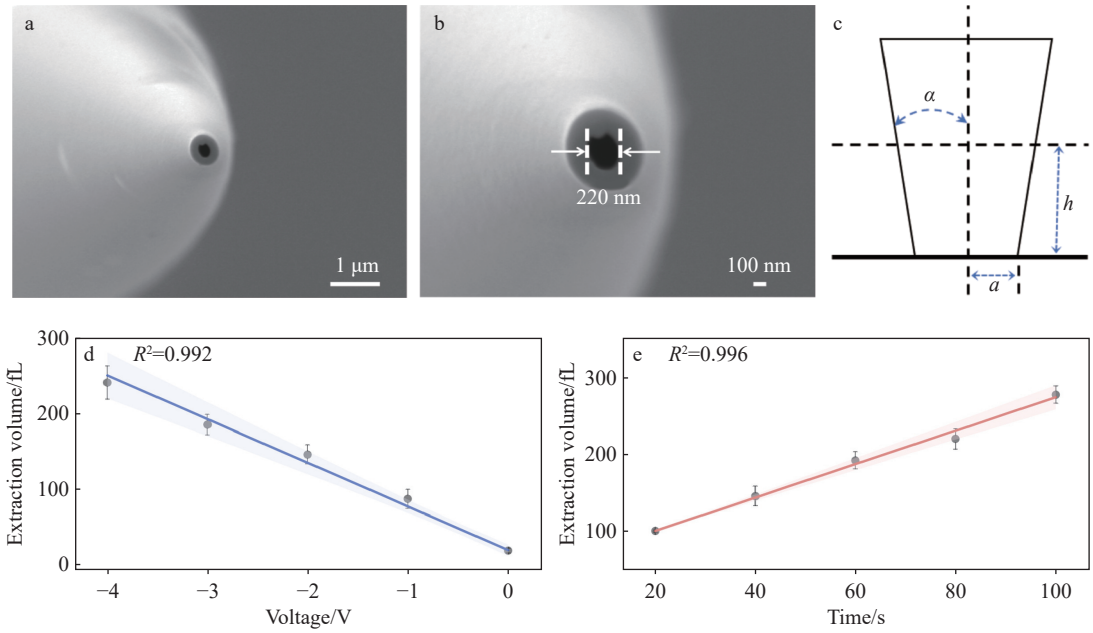

a. SEM images of the nanopipette; b. Enlarged view of panel A; c. Schematic diagram of the nanopipette tip model used for volume calculation; d. Linear relationship between sampling volume and sampling voltage at a fixed sampling time; e. Linear relationship between sampling volume and sampling time at a fixed sampling voltage

Fig. 2 SEM images of the nanopipette and optimization diagrams of electro-osmotic sampling

the optimal sampling condition was determined to be –2 V for 60 s, under which the estimated extraction volume from a single cell was approximately 190 fL.

Following extraction, the nanopipette was promptly transferred to the MS inlet. A high voltage (typically 2.5 kV) was applied to the rear of the capillary to induce stable electrospray, allowing the analytes to be ionized and introduced into the mass spectrometer in the gas phase. Using the single-cell quantitative MS platform, quantification of intracellular metabolites was achieved.

2.2　Development of a MS Method for Detecting TCA Cycle Metabolites

In general, the TCA cycle is a central metabolic pathway in cells that breaks down carbohydrates, fatty acids, and other molecules to produce energy required for cellular activities. The TCA cycle begins with acetyl-CoA combining with oxaloacetate to form citrate. Citrate is converted to isocitrate through aconitate, which is then transformed into *α*-ketoglutarate. *α*-Ketoglutarate is further converted to succinate, followed by oxidation to fumarate. Fumarate is hydrated to malate, which is finally oxidized back to oxaloacetate, completing the cycle. These key metabolites, including citrate, aconitate, isocitrate, *α*-ketoglutarate, succinate, fumarate, malate, and oxaloacetate, play important roles in energy metabolism and biosynthesis. During this cycle, the metabolites not only contribute to energy production but also participate in various other cellular processes. In the development of drug resistance, a number of metabolites in the TCA cycle have been revealed to contribute to this phenomenon, such as citrate, isocitrate, *α*-ketoglutarate, succinate, fumarate, malate, and oxaloacetate. Therefore, the single-cell analysis of these metabolites may provide valuable insights into the metabolic state and functional changes that occur within cells.

To achieve quantitative detection of these metabolites, MRM mode was employed and precursor ions (Q1) and product ions (Q3) were assigned to each metabolite. The parameters such as collision energy (CE) and declustering potential (DP) were systematically optimized to maximize signal response and detection sensitivity, ensuring accuracy and reproducibility in quantification. Finally, two high-response transitions for each metabolite were ultimately selected as the detection channels to achieve stronger detection signals. The MRM transition parameters for metabolites detected under positive ion mode are listed in Table 1, while those for metabolites detected under negative ion mode are listed in Table 2. It is worth noting that chromatographic separation was not introduced in this single-cell detection method. As a result, metabolite isomers with the same precursor and product ions cannot be effectively distinguished, such as citrate and isocitrate. Therefore, the signals of citrate and isocitrate were combined and quantified together as a single "citrate/isocitrate" measure. After the MRM method was established, it was applied to the analysis of standard compounds. As shown in Fig.3, all target metabolites were successfully detected. To enable quantitative analysis, we introduced 4-acetaminophen as an internal standard, a compound that does not naturally occur in the organism and exhibits a strong mass spectrometric response.

Quantitative analysis of metabolites was performed by integrating the peak areas of metabolites and the internal standard. Using 5% BSA

Table 1　MRM transitions for metabolite detection under positive ion mode on the single-cell quantitative MS platform

Metabolite	Q1(*m*/*z*)	Q3(*m*/*z*)	Dwell time/ ms	DP*/V	CE*/V
Aconitate	175.2	43.0	8	80	39.7
	175.2	69.0	8	80	30.6
	175.2	83.1	8	80	24.9
Citrate/Isocitrate	193.0	69.0	8	80	21.0
	193.0	87.0	8	80	21.0
	193.0	101.0	8	80	21.0
Oxaloacetate	133.1	44.8	8	80	24.9
	133.1	72.9	8	80	13.4
	133.1	105.1	8	80	22.6

*DP: declustering potential; CE: collision energy

Table 2 MRM transitions for metabolite detection under negative ion mode on the single-cell quantitative MS platform

Metabolite	Q1(*m*/*z*)	Q3(*m*/*z*)	Dwell time/ms	DP*/V	CE*/V
Fumarate	114.9	45.2	8	−80	−40.0
	114.9	71.1	8	−80	−10.2
Malate	133.0	57.1	8	−80	−20.0
	133.0	72.9	8	−80	−23.1
	133.0	74.9	8	−80	−17.0
Succinate	116.9	57.1	8	−80	−15.0
	116.9	73.0	8	−80	−14.9
	116.9	99.2	8	−80	−15.9
α-Ketoglutarate	144.8	57.1	8	−80	−15.9
	144.8	73.1	8	−80	−14.3
	144.8	100.7	8	−80	−11.3

*DP: declustering potential; CE: collision energy

as a surrogate matrix, we experimentally determined the limit of detection (LOD), LLOQ, and linear range for each metabolite. In addition, the LLOQ concentration of each metabolite was used as the QC level to evaluate the accuracy and precision of the method. The results showed that both intra-day and inter-day precision were within ±20%, meeting the standard methodological requirements[31]. Furthermore, the calibration curves for the metabolites are presented in Table 3, which demonstrate good linearity and suitability for analytical detection.

2.3 Detection of Metabolites in MCF-7 and MCF-7/ADR Cells

Based on the aforementioned method, single-cell analysis was conducted on MCF-7 breast cancer cells and their DOX-resistant counterpart, MCF-7/ADR. After sample size estimation, 60 individual cells were analyzed per group. A representative image of the single-cell sampling process is shown in Fig.4. A comparative analysis of the metabolic profiles between MCF-7 cells and MCF-7/ADR cells revealed a notable shift in the levels of key TCA cycle metabolites. Specifically, metabolites associated with the middle and later stages of the TCA cycle including *α*-ketoglutarate, succinate, fumarate, and malate were significantly elevated in the drug-resistant cells. In contrast, early-stage metabolites such as citrate/isocitrate, oxaloacetate and aconitate remained relatively unchanged between the two cell lines (Fig.5). This observation suggests a selective enhancement of specific segments of the TCA cycle in drug-resistant cells, rather than a uniform upregulation of the entire pathway. Furthermore, as shown in Fig.6, heatmap-based hierarchical clustering and PCA demonstrated clear separation between the two cell groups, with the majority of cells correctly assigned to two distinct clusters. This differential metabolic profile suggests that drug-resistant breast cancer cells may not globally enhance the activity of the entire TCA cycle, but rather selectively reprogram metabolism by emphasizing the middle and downstream segments.

In addition, notable variations in the abundance of the metabolites in individual cells were observed across the two cell lines. Using the 95% confidence interval (CI) derived from the MCF-7 cell group as a

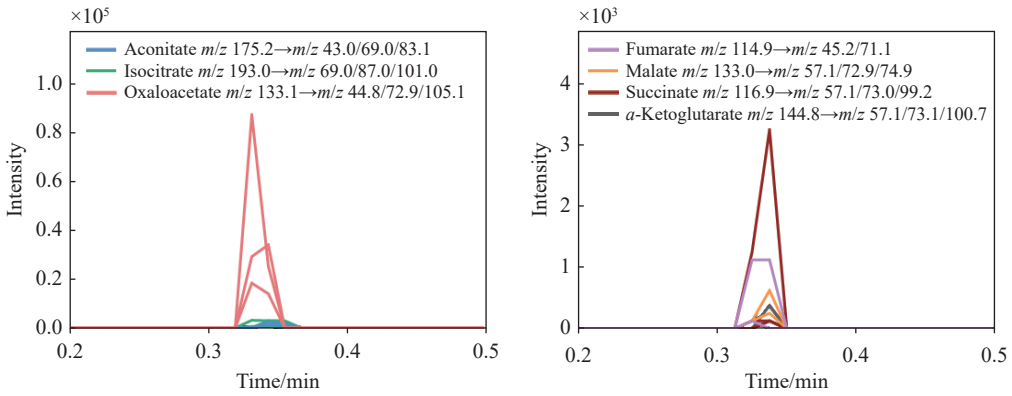

Fig. 3 Mass spectra of the metabolites detected on the single-cell quantitative MS platform

Table 3　Validation of MS-based single-cell quantitative analysis of metabolites

Metabolite	Linear range/(mmol/L)	Linear equation*	R^2	LOD/(mmol/L)	LLOQ/(mmol/L)	Bias/%	Intra-day precision (*CV*/%)	Inter-day precision (*CV*/%)
Citrate/Isocitrate	0.5-10.0	lg(*y*)=1.038·lg(*x*)−0.129	0.98	0.05	0.5	5.2	11.1	15.2
Oxaloacetate	1.0-20.0	lg(*y*)=1.125·lg(*x*)−0.032	0.96	0.05	1.0	3.5	12.7	13.3
Aconitate	0.01-1.00	lg(*y*)=0.987·lg(*x*)−1.378	0.96	0	0.01	−4.5	14.5	12.4
α-Ketoglutarate	0.5-10.0	lg(*y*)=1.234·lg(*x*)−0.126	0.98	0.01	0.5	6.8	12.9	11.4
Succinate	0.5-10.0	lg(*y*)=0.995·lg(*x*)−0.576	0.96	0.01	0.5	5.1	9.8	11.6
Fumarate	0.01-5.00	lg(*y*)=1.097·lg(*x*)−1.113	0.97	0.001	0.01	−5.2	14.5	16.3
Malate	1.0-20.0	lg(*y*)=1.525·lg(*x*)−1.294	0.96	0.05	1.0	6.1	12.4	11.6

*x: metabolite concentration; y: area ratio

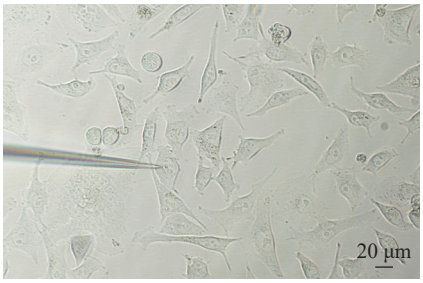

Fig. 4　Bright-field image of a nanopipette inserted into a single-cell for microsampling

reference, we evaluated the deviation between MCF-7/ADR cells and MCF-7 cells at single-cell resolution. For citrate/isocitrate, oxaloacetate and aconitate, a significant portion of MCF-7/ADR cells (15.0%, 21.7% and 18.3%) exhibited their levels higher than the reference CI interval of MCF-7 cells, indicating that not all MCF-7/ADR cells deviate equally from the metabolic profile of the parental line in these particular metabolites. Furthermore, this result can clearly show the distribution of metabolite concentrations, revealing the differences between two cell lines at the single-cell level, rather than just comparing average values. In addition, *α*-ketoglutarate, succinate, fumarate and malate were significantly elevated in the resistant cells. Comparatively, for malate and fumarate, the differences were more pronounced. All the MCF-7/ADR cells had their concentrations higher than the reference CI interval of MCF-7 cells. This fact suggests that malate and fumarate may reflect more stable or prominent metabolic changes associated

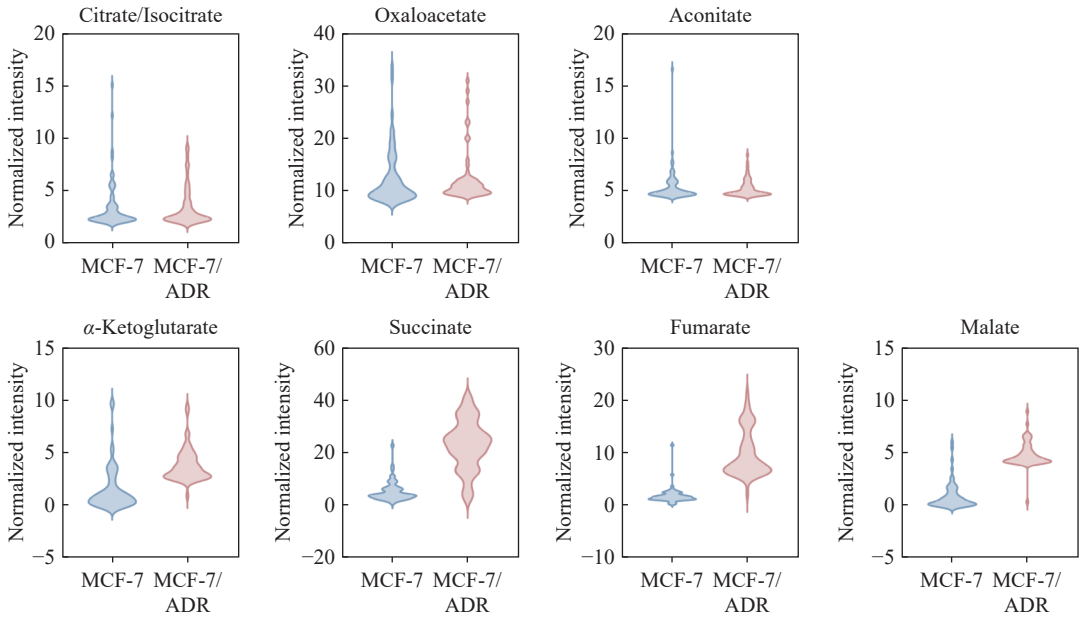

Fig. 5　Relative abundance of TCA cycle metabolites in single MCF-7 and MCF-7/ADR cells

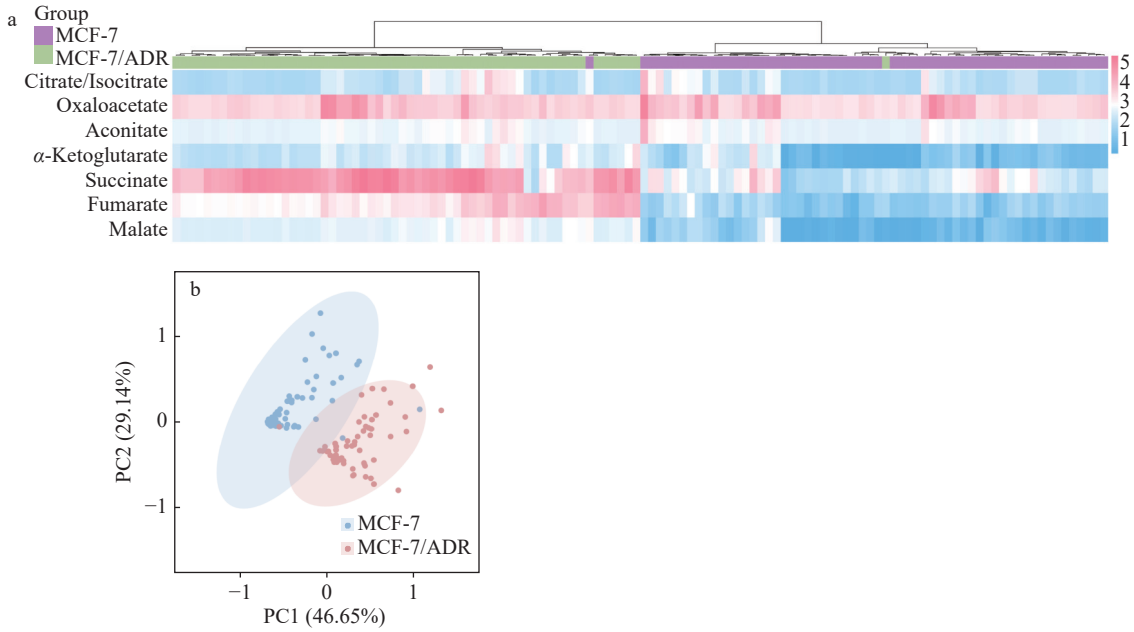

Fig. 6 Heatmap clustering analysis (a) and PCA analysis (b) based on the abundance of TCA cycle metabolites in single MCF-7 and MCF-7/ADR cells

with resistance. These results cannot be easily revealed by bulk analyses that usually obtain average signals across many cells.

The elevated level of α-ketoglutarate, a central node of glutaminolysis, indicates that drug-resistant cells may rely more heavily on the "glutamine-α-ketoglutarate" axis to fuel the TCA cycle and support nitrogen and energy demands. The accumulation of succinate and fumarate may reflect enhanced activity of succinate dehydrogenase and fumarase, respectively, which promotes downstream NADH generation and drives mitochondrial oxidative phosphorylation, supporting cell survival and anabolic processes under drug-induced stress[32]. Additionally, increased levels of malate may help maintain the cellular redox balance by regulating the NAD^+/NADH ratio, providing antioxidant capacity and protecting against DOX-induced oxidative damage. To better illustrate the metabolic shift observed here, the expression levels of isocitrate dehydrogenase 1 (IDH1) and glutaminase (GLS), which are responsible for the generation of α-ketoglutarate, were evaluated in MCF-7 and MCF-7/ADR cells by Western blotting (Fig.7a). As expected, there was a significant increase in the expression of IDH1 and GLS in MCF-7/ADR cells. By integrating the results above, a schematic representation of the metabolic processes associated with the drug resistance in MCF-7/ADR cells is shown in Fig.7b.

Interestingly, the levels of early-stage metabolites such as citrate/isocitrate remained relatively unchanged. As citrate also serves as a key precursor for fatty acid and cholesterol biosynthesis, its steady-state concentration may be influenced by substrate availability, enzyme activity regulation, or feedback inhibition. It is also possible that citrate is rapidly diverted to other branches of metabolism, such as lipid synthesis or histone acetylation pathways, thereby preventing its accumulation in the TCA cycle. The regulation of isocitrate dehydrogenase may also play a role in this process, though the precise mechanism warrants further investigation[33].

It is worth mentioning that the observed metabolic profiles may offer valuable insights into reversing drug resistance in clinical settings. As described above, there was an enhanced glutaminolysis in some DOX-resistant cancer cells. Therefore, combination of glutaminase inhibitors

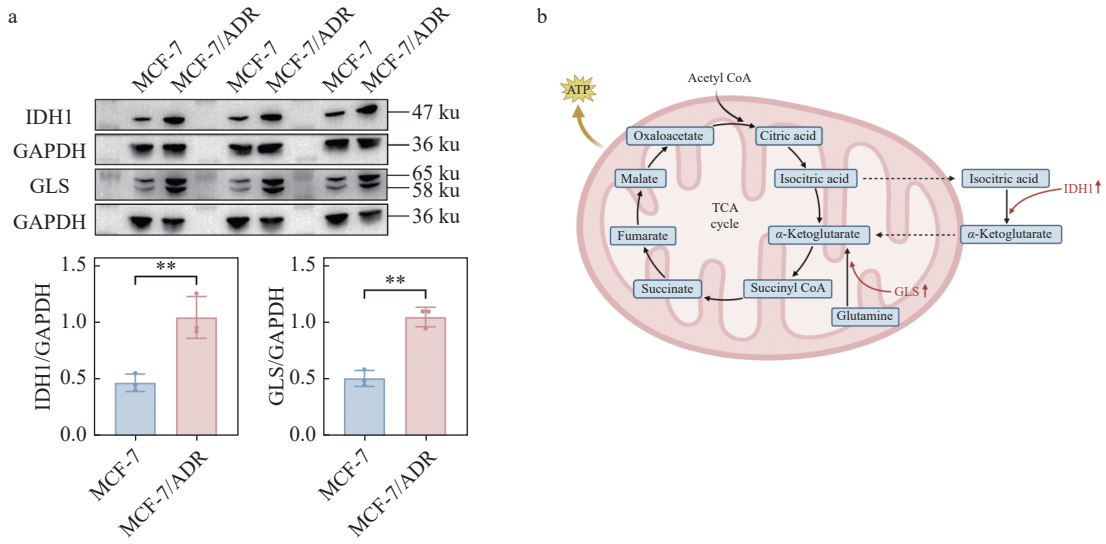

GAPDH was used as an internal reference; Data were analyzed with Student's t test, $^{**}p<0.01$

Fig. 7　Western blotting and the corresponding normalized analysis of IDH1 and GLS in MCF-7 and MCF-7/ADR cells (a), schematic representation of the metabolic processes associated with drug resistance in MCF-7/ADR cells (b)

with DOX for the treatment of DOX-resistant breast cancer may achieve potential synergistic benefits. Consistent with this speculation, recent preclinical studies demonstrated that glutaminase inhibitor CB-839 can reduce glutathione synthesis and increase oxidative stress, thereby sensitizing DOX-resistant cells to DOX. In addition, there is evidence also indicating that combining CB-839 with DOX can significantly inhibit tumor growth compared to monotherapy, highlighting the potential of this combinational approach[34-35].

Taken together, these findings suggest that the acquisition of DOX resistance in breast cancer cells is accompanied by a selective reprogramming of TCA cycle metabolism, particularly enhancing mitochondrial function at the middle and late stages. The metabolic heterogeneity in cells can stem from the underlying physiological differences such as variations in mitochondrial function and lipid uptake and composition[36], and further contribute to the step wise acquisition of DOX resistance, where more metabolically divergent cells may acquire stronger DOX resistance earlier[37-38]. Specifically, cells with mild metabolic shifts, such as slightly elevated reactive oxygen species (ROS) handling capacity or modest alterations in lipid metabolism, may survive initial drug exposure, while cells with more pronounced metabolic remodeling gradually emerge under continued selective pressure. Such progressive enrichment of metabolically divergent subgroups facilitates a continuum from partial tolerance to full resistance. On the other hand, cell subgroups with distinct metabolic states linked to lower response to DOX can be identified, enabling a more precise understanding of drug resistance mechanisms and potentially guiding targeted therapeutic strategies that bulk methods would overlook.

3　Conclusion

In conclusion, this study successfully utilized a home-built single-cell quantitative MS platform for profiling metabolites at the single-cell level. Distinct metabolic profiles in single drug-resistant cancer cells were discovered. The observed selective upregulation of downstream TCA cycle metabolites is well consistent with the physiological differences in energy production and oxidative stress during drug resistance acquisition. In addition to the observed cellular metabolic heterogeneity in these drug-resistant cells, how the metabolic profiles differ from

those of their parental counterparts and thus the extent of metabolic deviation are also demonstrated. In the future, the relationship between physiological differences, metabolic heterogeneity, and differential drug resistance acquisition could be further understood through comprehensive mechanism studies. Additionally, the step wise development of drug resistance may be better tracked by focusing on the cell subgroups with distinct metabolic states linked to lower response to drugs and using longitudinal monitoring approaches. Such investigations would help distinguish key metabolic contributors to chemotherapy resistance, potentially guiding the discovery of targeted therapeutic strategies. In principle, the approach developed in this study can be applied to investigate other metabolic processes and their associated cell types.

References:

[1] KIM J, HARPER A, MCCORMACK V, SUNG H, HOUSSAMI N, MORGAN E, MUTEBI M, GARVEY G, SOERJOMATARAM I, FIDLER-BENAOUDIA M M. Global patterns and trends in breast cancer incidence and mortality across 185 countries[J]. Nat Med, 2025, 31(4): 1 154-1 162.

[2] OBEAGU E I, OBEAGU G U. Breast cancer: a review of risk factors and diagnosis[J]. Medicine, 2024, 103(3): e36905.

[3] TRAYES K P, COKENAKES S E. Breast cancer treatment[J]. American family physician, 2021, 104(2): 171-178.

[4] WAKS A G, WINER E P. Breast cancer treatment: a review[J]. The Journal of the American Medical Association, 2019, 321(3): 288-300.

[5] PILCO-FERRETO N, CALAF G M. Influence of doxorubicin on apoptosis and oxidative stress in breast cancer cell lines[J]. International Journal of Oncology, 2016, 49(2): 753-762.

[6] IBRAHIM N K, FRYE D K, BUZDAR A U, WALTERS R S, HORTOBAGYI G N. Doxorubicin-based chemotherapy in elderly patients with metastatic breast cancer. Tolerance and outcome[J]. Archives of Internal Medicine, 1996, 156(8): 882-888.

[7] LOVITT C J, SHELPER T B, AVERY V M. Doxorubicin resistance in breast cancer cells is mediated by extracellular matrix proteins[J]. BMC Cancer, 2018, 18(1): 41.

[8] PONNUSAMY L, MAHALINGAIAH P K S, SINGH K P. Treatment schedule and estrogen receptor-status influence acquisition of doxorubicin resistance in breast cancer cells[J]. European Journal of Pharmaceutical Sciences, 2017, 104: 424-433.

[9] FAUBERT B, SOLMONSON A, DeBERARDINIS R J. Metabolic reprogramming and cancer progression[J]. Science, 2020, 368(6 487): eaaw5473.

[10] GANDHI N, DAS G M. Metabolic reprogramming in breast cancer and its therapeutic implications[J]. Cells, 2019, 8(2): 89.

[11] VASAN N, BASELGA J, HYMAN D M. A view on drug resistance in cancer[J]. Nature, 2019, 575(7 782): 299-309.

[12] GUPTA R, GUPTA N, GUPTA R. Tricarboxylic acid cycle[J]. Fundamentals of Bacterial Physiology and Metabolism, 2021: 327-346.

[13] ENIAFE J, JIANG S. The functional roles of TCA cycle metabolites in cancer[J]. Oncogene, 2021, 40(19): 3 351-3 363.

[14] WU J, LIU N, CHEN J, TAO Q, LI Q, LI J, CHEN X, PENG C. The tricarboxylic acid cycle metabolites for cancer: friend or enemy[J]. Research, 2024, 7: 0 351.

[15] RAHMAN M, HASAN M R. Cancer metabolism and drug resistance[J]. Metabolites, 2015, 5(4): 571-600.

[16] ANDERSON N M, MUCKA P, KERN J G, FENG H. The emerging role and targetability of the TCA cycle in cancer metabolism[J]. Protein & Cell, 2018, 9(2): 216-237.

[17] YANG J, CHENG R, PAN X, PAN S, DU M, YAO H, HU Z, ZHANG S, ZHANG X. Single-cell unsaturated lipid profiling for studying chemoresistance heterogeneity of triple-negative breast cancer cells[J]. Analytical Chemistry, 2024, doi: 10.1021/acs.analchem.3c04887.

[18] AMIRI-D N, YEKTA R F, KOUSHKI M, AREFI O A, ESFAHANI H, TAHERI S, KAZEMIAN E. Metabolomic study of serum in patients with invasive ductal breast carcinoma with LC-MS/MS approach[J]. The International Journal of Biological Markers, 2022, 37(4): 349-359.

[19] ESTRADA-PÉREZ A R, ROSALES-HERNÁNDEZ M C, GARCÍA-VÁZQUEZ J B, BAKALARA N, FROMAGER B, CORREA-BASURTO J. Untargeted LC-MS/MS metabolomics study on the MCF-7 cell line in the presence of valproic acid[J]. International Journal of Molecular Sciences, 2022, 23(5): 2 645.

[20] ZHANG L, VERTES A. Single-cell mass spectrometry

approaches to explore cellular heterogeneity[J]. Angewandte Chemie International Edition, 2018, 57(17): 4 466-4 477.

[21] TAJIK M, BAHARFAR M, DONALD W A. Single-cell mass spectrometry[J]. Trends in Biotechnology, 2022, 40(11): 1 374-1 392.

[22] PAN R, XU M, JIANG D, BURGESS J D, CHEN H Y. Nanokit for single-cell electrochemical analyses[J]. Proceedings of the National Academy of Sciences of the United States of America, 2016, 113(41): 11 436-11 440.

[23] AMANN R, FUCHS B M. Single-cell identification in microbial communities by improved fluorescence *in situ* hybridization techniques[J]. Nature Reviews Microbiology, 2008, 6(5): 339-348.

[24] ZHU G, SHAO Y, LIU Y, PEI T, LI L, ZHANG D, GUO G, WANG X. Single-cell metabolite analysis by electrospray ionization mass spectrometry[J]. TrAC Trends in Analytical Chemistry, 2021, 143: 116 351.

[25] XU X, JIANG X, SHI M, YIN L. Mass spectrometry-based techniques for single-cell analysis[J]. The Analyst, 2023, 148(16): 3 690-3 707.

[26] QIN S, MIAO D, ZHANG X, ZHANG Y, BAI Y. Methods developments of mass spectrometry based single cell metabolomics[J]. TrAC Trends in Analytical Chemistry, 2023, 164: 117 086.

[27] XU T, FENG D, LI H, HU X, WANG T, HU C, SHI X, XU G. Recent advances and typical applications in mass spectrometry-based technologies for single-cell metabolite analysis[J]. TrAC Trends in Analytical Chemistry, 2022, 157: 116 763.

[28] ZHANG W, XU F, YAO J, MAO C, ZHU M, QIAN M, HU J, ZHONG H, ZHOU J, SHI X, CHEN Y. Single-cell metabolic fingerprints discover a cluster of circulating tumor cells with distinct metastatic potential[J]. Nature Communications, 2023, 14(1): 2 485.

[29] CALCAGNO A M, SALCIDO C D, GILLET J P, WU C P, FOSTEL J M, MUMAU M D, GOTTESMAN M M, VARTICOVSKI L, AMBUDKAR S V. Prolonged drug selection of breast cancer cells and enrichment of cancer stem cell characteristics[J]. Journal of the National Cancer Institute, 2010, 102(21): 1 637-1 652.

[30] LAFORGE F O, CARPINO J, ROTENBERG S A, MIRKIN M V. Electrochemical attosyringe[J]. Proceedings of the National Academy of Sciences of the United States of America, 2007, 104(29): 11 895-11 900.

[31] ZENOBI R. Single-cell metabolomics: analytical and biological perspectives[J]. Science, 2013, 342(6 163): 1 243 259.

[32] GAUDE E, FREZZA C. Defects in mitochondrial metabolism and cancer[J]. Cancer & Metabolism, 2014, 2: 10.

[33] LIU Y, XU W, LI M, YANG Y, SUN D, CHEN L, LI H, CHEN L. The regulatory mechanisms and inhibitors of isocitrate dehydrogenase 1 in cancer[J]. Acta Pharmaceutica Sinica B, 2023, 13(4): 1 438-1 466.

[34] LE A, LANE A N, HAMAKER M, BOSE S, GOUW A, BARBI J, TSUKAMOTO T, ROJAS C J, SLUSHER B S, ZHANG H, ZIMMERMAN L J, LIEBLER D C, SLEBOS R J C, LORKIEWICZ P K, HIGASHI R M, FAN T W M, DANG C V. Glucose-independent glutamine metabolism *via* TCA cycling for proliferation and survival in B cells[J]. Cell Metabolism, 2012, 15(1): 110-121.

[35] GROSS M I, DEMO S D, DENNISON J B, CHEN L, CHERNOV-ROGAN T, GOYAL B, JANES J R, LAIDIG G J, LEWIS E R, LI J, MacKINNON A L, PARLATI F, RODRIGUEZ M L M, SHWONEK P J, SJOGREN E B, STANTON T F, WANG T, YANG J, ZHAO F, BENNETT M K. Antitumor activity of the glutaminase inhibitor CB-839 in triple-negative breast cancer[J]. Molecular Cancer Therapeutics, 2014, 13(4): 890-901.

[36] AZAM A, SOUNNI N E. Lipid metabolism heterogeneity and crosstalk with mitochondria functions drive breast cancer progression and drug resistance[J]. Cancers, 2022, 14(24): 6 267.

[37] MATHIS R A, SOKOL E S, GUPTA P B. Cancer cells exhibit clonal diversity in phenotypic plasticity[J]. Open Biology, 2017, 7(2): 160 283.

[38] KEMPER K, de GOEJE P L, PEEPER D S, van AMERONGEN R. Phenotype switching: tumor cell plasticity as a resistance mechanism and target for therapy[J]. Cancer Research, 2014, 74(21): 5 937-5 941.

（Received date: 2025-06-15; Revised date: 2025-10-14）